,

Evidence for the Onset of Deconfinement and Quest for the Critical Point by NA49 at the CERN SPS

G. L. Melkumov (for the NA49 Collab.),[1,*] T. Anticic,[2] B. Baatar,[1] D. Barna,[3] J. Bartke,[4] H. Beck,[5] L. Betev,[6] H. Białkowska,[7] C. Blume,[5] M. Bogusz,[8] B. Boimska,[7] J. Book,[5] M. Botje,[9] P. Bunčić,[6] T. Cetner,[8] P. Christakoglou,[9] P. Chung,[10] O. Chvala,[11] J. G. Cramer,[12] V. Eckardt,[13] Z. Fodor,[3] P. Foka,[14] V. Friese,[14] M. Gaździcki,[5,15] K. Grebieszkow,[8] C. Höhne,[14] K. Kadija,[2] A. Karev,[6] V. I. Kolesnikov,[1] T. Kolleger,[5] M. Kowalski,[4] D. Kresan,[14] A. Laszlo,[3] R. Lacey,[10] M. van Leeuwen,[9] M. Mackowiak,[8] M. Makariev,[16] A. I. Malakhov,[1] M. Mateev,[17] M. Mitrovski,[5] St. Mrówczyński,[15] N. Nicolic,[2] G. Pálla,[3] A. D. Planagiotou,[18] W. Peryt,[8] J. Pluta,[8] D. Prindle,[12] F. Pühlhofer,[19] R. Renfordt,[5] C. Roland,[20] G. Roland,[20] M. Rybczyński,[15] A. Rybicki,[4] A. Sandoval,[14] N. Schmitz,[13] T. Schuster,[5] P. Seyboth,[13] F. Siklér,[3] E. Skrzypczak,[21] M. Slodkowski,[8] G. Stefanek,[15] R. Stock,[5] H. Ströbele,[5] T. Susa,[2] M. Szuba,[8] M. Utvić,[5] D. Varga,[22] M. Vassiliou,[18] G. I. Veres,[3] G. Vestergombi,[3] D. Vranić,[14] Z Włodarczyk,[15] and A. Wojtaszek-Szwarc[15]

[1] *Joint Institute for Nuclear Research, Dubna, Russia.*

[2] *Rudjer Boskovic Institute, Zagreb, Croatia.*

[3] *KFKI Research Institute for Particle and Nuclear Physics, Budapest, Hungary.*

[4] *H. Niewodniczański Institute of Nuclear Physics, Polish Academy of Sciences, Cracow, Poland.*

[5] *Fachbereich Physik der Universität, Frankfurt, Germany.*

[6] *CERN, Geneva, Switzerland.*

[7] *Institute for Nuclear Studies, Warsaw, Poland.*

[8] *Faculty of Physics, Warsaw University of Technology, Warsaw, Poland.*

[9] *NIKHEF, Amsterdam, Netherlands.*

[10] *Department of Chemistry, Stony Brook Univ. (SUNYSB), Stony Brook, USA.*

[11] *Inst. of Particle and Nuclear Physics, Charles Univ., Prague, Czech Republic.*

[12]*Nuclear Physics Laboratory, University of Washington, Seattle, WA, USA.*

[13]*Max-Planck-Institut für Physik, Munich, Germany.*

[14]*Gesellschaft für Schwerionenforschung (GSI), Darmstadt, Germany.*

[15]*Institute of Physics Świ etokrzyska Academy, Kielce, Poland.*

[16]*Institute for Nuclear Research and Nuclear Energy, Sofia, Bulgaria.*

[17]*Atomic Physics Department, Sofia Univ. St. Kliment Ohridski, Sofia, Bulgaria.*

[18] *Department of Physics, University of Athens, Athens, Greece.*

[19]*Fachbereich Physik der Universität, Marburg, Germany.*

[20]*MIT, Cambridge, USA.*

[21]*Institute for Experimental Physics, University of Warsaw, Warsaw, Poland.*

[22]*Eötvös Loránt University, Hungary.*

The NA49 results on hadron production obtained in PbPb collisions at SPS energies from 20 AGeV to 158 AGeV are shown and discussed as evidence for the onset of deconfinement. The primary measures are the pion yield, the kaon to pion ratio and the slope parameter of transverse mass distributions.

The possible indication of the QCD critical point signatures was investigated in the event-by-event fluctuations of various observables such as the mean transverse momentum, particle multiplicity and azimuthal angle distributions as well as in the particle ratio fluctuations. The energy dependence of these observables was measured in central PbPb collisions in the full SPS energy range while for analysis of the system size dependence data from *pp*, CC, SiSi, and PbPb collisions at the top SPS energy were used.

1. INTRODUCTION

It was early shown [1] that nucleus-nucleus collisions at the CERN SPS offered the possibility of reaching energy densities in excess of about 1 GeV/fm^3 during the early stage of the reaction. Under these conditions QCD predicts a phase transition between hadronic matter and state of quasifree quarks and gluons called the quark-gluon plasma (QGP).

* Electronic address: Georgui.Melkoumov@cern.ch

Indeed, the predicted signatures of the QGP, e.g. strangeness enhancement, charmonia suppression, and dilepton enhancement were observed in PbPb collisions at the top SPS energy ($\sqrt{s_{NN}}$ = 17.3 GeV). Following these observations of a new state of matter [2], the energy dependence of inclusive hadronic observables, i.e. the K/π ratio, the total pion yield, and the slope parameter of hadron transverse momentum spectra gave evidence that the predicted signatures of the onset of deconfinement transition [3] is observed at low SPS energies around $\sqrt{s_{NN}}$ = 8 GeV [4–7]. Final results from these studies will be reviewed.

Further insight into the early stage of nucleus-nucleus collisions was motivated by predictions from modern lattice QCD and the QCD model calculations indicating the primaty features of the phase diagram of strongly interacting matter (Fig. 1*a*). The QCD suggests that deconfined matter (QGP) is separated from hadron phase, hadron gas (HG), by a first order transition boundary at large bario-chemical potential μ_B ending in a critical point E and then turning into a cross-over transition at low values of μ_B (low baryon density). A recent extension to the finite μ_B domain allowed to estimate the position of the critical point E [8].

The location of the hadron chemical freeze-out points of the high density fireball produced in nucleus-nucleus collisions is shown in Fig. 1*a*. They are obtained from fits of a statistical hadron gas model to hadron abundandances [9–11]. It provides a good fit to the total yields of numerous particle species with 3 parametrs, namely a temperature T, a baryochemical potential μ_B, and a strangeness saturation parameter γ_s (Fig. 1*b*). The resulting freeze-out points for central PbPb collisions in the CERN SPS energy range are seen to approach the estimated phase boundary and the critical point E.

In the vicinity of the QCD critical point a large event-by-event fluctuations of various observables are expected [12, 13]. This paper reports the status of the search for such fluctuations. Results will be presented from analysis of central PbPb collisions, which were recorded for SPS beam energies of 20, 30, 40, 80, and 158 AGeV ($\sqrt{s_{NN}}$ = 6.3, 7.6, 8.7, 12.3, and 17.3 GeV) as well as from *pp*, CC and SiSi interactions at 158 AGeV.

2. EXPERIMENT

The experiment was carried out with the NA49 large acceptance hadron detector [14] employing a system of time projection chambers (TPCs) for efficient tracking in the forward

hemisphere of the reactions, precise momentum reconstruction in the magnetic field, and particle identification using the energy loss dE/dx in the TPC gas. Two time of flight (TOF) walls of 900 scintillator pixels each situated symmetrically behined TPCs augment particle identification near midrapidity. A zero degree calorimeter ZDC is used for centrality selection of events in nucleus -nucleus collisions at triggering as well as in the off-line analysis.

Raw charged particle yields were obtained by unfolding the distributions of dE/dx and from TOF measurements in small bins of momentum p and transverse momentum p_t. Strange particles (K^0_S, Λ, Ξ, Ω) are detected via decay topology and invariant mass measurement. A various type of corrections have been applied to the data, such as corrections for geometrical acceptance, reconstruction efficiency, in-flight particle decay, and feeddown from weak decays.

3. ONSET OF DECONFINEMENT

There is a firm notion that in central collisions of heavy nuclei at the top SPS energy ($\sqrt{s_{NN}}$ = 17.3 GeV) as well as at RHIC energies ($\sqrt{s_{NN}}$ = 130 and 200 GeV) a transient state of deconfined quarks and gluons (QGP) is produced. It is argued by the observation of the signatures predicted for the QGP. Moreover, in the phase diagram of strongly interacting matter, the hadronic final states of such collisions analysed in the framework of the statistical hadron gas model are close to the phase boundary predicted by the lattice QCD calculations.

In order to find out whether the early stage fireball actually reaches hadron deconfinement the energy dependence of the hadron production properties was studied. This program was originally motivated by the predictions of the Statistical Model of the Early Stage (SMES) [3] assuming that the energy threshold for deconfinement is located at low SPS energies. Several features were expected within this model, namely the "kink" in pion production, the "horn" in strangeness to entropy ratio, and the "step" in the inverse slope parameter of the transverse momentum spectra.

Fig. 2a shows the pion yield in full phase space of central PbPb collisions, normalized to the number of wounded nucleons N_w as a function of the collision energy expressed in a Fermi variable

$$F = (\sqrt{s_{NN}} - 2m_N)^{3/4}/\sqrt{s^{1/2}_{NN}} \approx \sqrt{s^{1/2}_{NN}}\,. \qquad (1)$$

The pions are the most abundantly produced particle species, therefore they measure the early stage entropy density created in the system as it stated in a statistical model approach. Compared to the same data in *pp* interaction one can see that the energy dependence of the pion yield in AA collisions changes its behaviour in the SPS energy region. It clearly steepens at low energies around 30 AGeV and can be interpreted as an increase of the number of effective degrees of freedom [3] by a factor ≈ 3 [4]. Such an increase may be considered as a consequence of the activation of partonic degrees of freedom when going from hadron gas to QGP.

Another formidable observation is a pronounced sharp maximum of K^+/π^+ ratio in central PbPb collisions at about 30 AGeV presented in Fig. 2*b*. It shows the K^+/π^+ ratio in a full phase space as a function of the collision energy [4]. The data are compared to the hadron-string transport models. This feature is not seen in *pp* interactions and not reproduced by the hadron-string models RQMD [15] , UrQMD [16], or HSD [17].

Since K^+ is by far the most abundant carrier of anti-strangeness at SPS energies, it provides a good measure of the total strangeness produced in the collisions. Thus, the K^+/π^+ ratio represents the strangeness to entropy ratio. A sharp maximum in this quantity was predicted by the SMES consideration as a consequence of the transition to a deconfined state [3]. The most relevant measure of the strangeness to entropy ratio used in this work is

$$E_S = (\langle \mathrm{K} + \bar{\mathrm{K}} \rangle + \langle \Lambda \rangle)/\langle \pi \rangle \tag{2}$$

calculated from π, K and Λ total yields in 4π acceptance. The energy dependence of E_S in central PbPb collisions is plotted in Fig. 2*c*. It exhibits a sharp peak at low SPS energy ($\sim$ 30 AGeV) with a fall-off to a lower plateau value consistent with expectation for a deconfined phase (dash-dotted curve). Upon the SMES consideration this is the result of the decrease of strangeness carrier mass in the QGP and the change in the number of degrees of freedom when reaching the deconfined state.

While discussing the excitation function of K/π ratio a special note should go to the hadron gas model (HGM), which is being successful in describing the final state of almost all hadron species. The HGM in its full equilibrium version [18] produces a broad maximum in K/π ratio and overestimates the relative kaon yields from $\sim$ 30 AGeV on. The latest extension of the HGM [19] manages a better description of these data. However, it relies on the unmeasured hadronic resonance states and the guessworked assumptions on their

branching ratios.

A phase transition is expected to also manifest itself in the momentum distributions. Fig. 3 shows the inverse slope parameters for K^+ and K^- [4] derived from transverse mass spectra of these particles at midrapidity as a function of the collision energies. One observes for slope parameter in AA collisions a steep rise at lower AGS energies turning into plateau over the entire SPS energy range and then gradually increasing towards RHIC energies. This structure is not seen in *pp* reactions and not reproduced by transport models UrQMD [16] and HSD [17].

Since the slope parameters measure both the local temperature and the pressure induced collective flow the step-like behavour observed for the kaon slopes is consistent with the constant temperature and pressure, the features peculiar for the mixed phase of a first-order phase transition. Indeed, a hydrodynamical model [20] incorporating a deconfimenent phase transition provides a satisfying description of the experimental data. The step-like behavior was shown [4] to be a characteristic feature also for pions, protons, and antiprotons.

Above feature attributed to the softest point of the equation of state as expected in the first order phase transition is also seen in the excitation function of sound velocity c_s [21], which has been derived from the width of the pion rapidity distributions of the NA49 using the Landau hydrodynamical model.

Finally, in conjunction with the transverse mass spectra, the fireball volume derived from the Bose-Einstein correlations allowed to extract the energy dependence the pion phase space density [22]. This quantity exhibits a plateau at SPS energies, which may also be related to the onset of deconfinement.

The NA49 data on hadron production at SPS energies have recently been confirmed by preliminary data from the STAR experiment at $\sqrt{s_{NN}} = 9.3$ and 19.6 GeV [23–25].

4. CRITICAL POINT AND PHASE TRANSITION EFFECTS IN FLUCTUATIONS

Experimental study of the predicted features of the phase diagram of strongly interacting matter such as the deconfinement transition and the critical point is the primary goal of a number of contemporary experiments, developing projects, and numerous theoretical investigations.

The QCD phase diagram [26] is often plotted in terms of temperature (T_{chem}) and bary-

ochemical potential (μ_B). The lattice QCD calculations indicate that at small chemical potential ($\mu_B \approx 0$) the transition from hadronic to partonic matter is a crossover [27], while at larger values of μ_B the transition becomes first order [28]. Therefore, one expects the existence of a critical point at the end of first order transition. Several lattice QCD calculations suggest the existence of the critical point (CP) of strongly interacting matter in the SPS energy range [8, 29]

One of the characteristic signatures of the critical point is an increase in fluctuations of various event-by-event observables, in particular the particle multiplicity and transverse momentum fluctuations [12, 13]. A signal of CP is expected to be maximal when freeze-out of the system created in the collision happens near critical point. These observations suggest that it might be possible to perform a 2-dimensional scan of the phase diagram of strongly interacting matter by changing $\sqrt{s_{NN}}$ (variation of μ_B) and the colliding system size A (variation of $T_{\rm chem}$) and look for a maximum of fluctuations as a signature for the critical point.

4.1. Transverse momentum and multiplicity fluctuations

In NA49 the Φ_{p_t} measure [30–32] and the scaled variance ω [33–35] are used for studying the mean transverse momentum and particle multiplicity fluctuations, respectively.

The definitions and properties of Φ_{p_t} and ω are important to briefly be specified, especially as Φ measure is employed in the analysis of fluctuations of the azimuthal particle distributions as well as the higher moments of mean p_t fluctuation to follow.

Upon the authors of [30], one can define the single-particle variable $z_{p_t} = p_t - \overline{p_t}$ with the bar denoting averaging over the single-particle inclusive distribution. As seen $\overline{z_{p_t}} = 0$. Further, the event variable Z_{p_t}, which is a multi-particle analog of z_{p_t}, defined as

$$Z_{p_t} = \sum_{i=1}^{N} (p_{ti} - \overline{p_t}), \tag{3}$$

where the summation runs over particles in a given event. Note, that $\langle Z_{p_t} \rangle = 0$, where $\langle ... \rangle$ represents averaging over events. Finally, the Φ_{p_t} measure is defined as

$$\Phi_{p_t} = \sqrt{\frac{\langle Z_{p_t}^2 \rangle}{\langle N \rangle}} - \sqrt{\overline{z_{p_t}^2}}. \tag{4}$$

So, the Φ_{p_t} measure represents the difference between the event average of a quantity $\langle p_t \rangle$ and its ensemble average.

For multiplicity fluctuation the scaled variance ω (variance of the multiplicity distribution normalized by its mean value) is defined as

$$\omega = \frac{\mathrm{Var}(n)}{\langle n \rangle} = \frac{\langle n^2 \rangle - \langle n \rangle^2}{\langle n \rangle} \,. \tag{5}$$

For a system of independently emitted particles (no inter-particle correlations) Φ_{p_t} is equal zero. For a Poisson multiplicity distribution ω equals 1. If AA reactions are a superposition of independent NN collisions then $\Phi_{p_t}(\mathrm{AA}) = \Phi_{p_t}(NN)$, whereas $\omega(\mathrm{AA}) = \omega(NN) + \langle n \rangle \omega_{\mathrm{part}}$, where $\langle n \rangle$ is the mean multiplicity of hadrons from a single NN collisions and ω_{part} represents fluctuations in the number of nucleons N_{part} participating in the collision. The above equations suggest that while Φ_{p_t} is independent of N_{part} fluctuations (intensive quantity), ω is strongly dependent on them (extensive quantity).

It is obvious, for the fluctuation studies one has to know the number of participating nucleons from the projectile ($N_{\mathrm{part}}^{\mathrm{proj}}$) and target ($N_{\mathrm{part}}^{\mathrm{targ}}$) nuclei with a high precision. In the NA49 fixed target experiment $N_{\mathrm{part}}^{\mathrm{proj}}$ can be fixed by means of the spectator energy measured in the Forward Calorimeter, whereas $N_{\mathrm{part}}^{\mathrm{targ}}$ cannot be measured. It was shown [36] that fluctuations of $N_{\mathrm{part}}^{\mathrm{targ}}$ can be suppressed only by selection of very central collisions. Therefore, the multiplicity fluctuations are presented for very central (1%) collisions.

The results of the NA49 study of transverse momentum [32] and multiplicity [34, 35] fluctuations are plotted in Figs. 4, 5, 6, and 7 [37, 38]. They present the energy (μ_B) and system size (T_{chem}) dependence of Φ_{p_t} and ω. The chemical freeze-out parameters, $T_{\mathrm{chem}}(\mathrm{A}, \sqrt{s_{NN}})$ and $\mu_B(\mathrm{A}, \sqrt{s_{NN}})$ were taken from fits of the hadron gas model [10] to particle yields. The lines correspond to predictions for critical points CP_1 and CP_2 with estimated magnitude of the effect for Φ_{p_t} and ω taken from [12, 39, 40], assuming correlation lenghts ξ decreases monotonicaly with decreasing system size (fireball), namely $\xi(\mathrm{PbPb}) = 6$ fm and $\xi(pp) = 2$ fm (dashed lines) or $\xi(\mathrm{PbPb}) = 3$ fm and $\xi(pp) = 1$ fm (solid lines). The expected magnitudes include NA49 corrections due to the limited forward rapidity range and the limited azimuthal angle acceptance of the detector.

As possible location of the critical point CP_1 the $\mu_B = 360$ MeV was taken from lattice QCD calculations [8] and the corresponding $T_{\mathrm{chem}} = 147$ MeV to be on the empirical freeze-out line for the 5 energies of central PbPb collisions.

For critical point CP_2 the measured chemical freeze-out parameters of pp reaction at 158 GeV, $\mu_B = 250$ MeV and $T_{\rm chem} = 178$ MeV, were suggested assuming that this point may be located on the phase transition line.

Figs. 4 and 5 show no significant energy dependence of mean p_t and multiplicity fluctuations at SPS energies. Thus the results do not provide evidence for for critical point CP_1 making possible conclusions that either the critical point is not close enough to manifest itself in the data or the correlation length realized in heavy ion collisions is very small.

The system size dependence of fluctuations presented in Figs. 6 and 7 exhibit a maximum of Φ_{p_t} and ω for intermediate systems CC and SiSi interactions at the top SPS energy. The peak is two times higher for all charged than for negatively charged particles as expected for the critical point [12]. Both figures suggest that the NA49 data are consistent with the CP_2 predictions. The prediction that the critical point effect would be twice as large in all charged particles than in only positive or negative particles is also consistent with the data.

It was expected [12] that fluctuations due to the critical point originate mainly from low p_t pions. Indeed, analysis of Φ_{p_t} at $0.005 < p_t < 1.5$ GeV/c shown [38] that fluctuations in high p_t region ($0.5 < p_t < 1.5$) are consistent with zero and correlations are observed predominantly at low p_t ($0.005 < p_t < 0.5$), which, however, do not show a maximum, but continuous rise towards PbPb collisions. The origin of this behavior still has to be understood.

4.2. Higher moments of transverse momentum fluctuations

Most fluctuation measures discussed to date can be related to a quadratic variances (second moments) of event-by-event observables, such as particle multiplicities, net charge, baryon number, particle ratios, or mean transverse momentum in the event. Typically, the singular contribution to quadratic variances of distributions induced by the proximity of the critical point is proportional to approximately ξ^2, where ξ is the correlation length.

For future fluctuation studies, higher moments of event-by-event distributions will be of great interest. It was pointed out [41–43] that higher moments of the fluctuations are much more sensitive to the proximity of the critical point than the commonly employed measures based on the quadratic measures. In this case the amplitude of the critical point peak became proportional to higher powers of the correlation length ξ. For example, the fourth and third

moments of the particle multiplicity distributions $\langle N^4 \rangle \sim \xi^7$ and $\langle N^3 \rangle \sim \xi^{4.5}$ should be compared to $\langle N^2 \rangle \sim \xi^2$ for second moment, respectively.

The first attempt of NA49 in studying the higher moment fluctuations was applied to the mean p_t observable using the Φ measure. In general case, the n-th moment is defined as

$$\Phi_{p_t}^{(n)} = \left(\frac{\langle Z_{p_t}^n \rangle}{\langle N \rangle} \right)^{1/n} - (\overline{z_{p_t}})^{1/n} \ . \tag{6}$$

In present analysis, the third moment $\Phi_{p_t}^{(3)}$ was employed because of its crucial advantages. As shown in theoretical study [41] the only $\Phi_{p_t}^{(3)}$, and not the higher moments, preserves the same properties of the second moment $\Phi_{p_t}^{(2)}$ for the source of independently emitted particles. It was also found that similarly to $\Phi_{p_t}^{(2)}$, the $\Phi_{p_t}^{(3)}$ is the intensive thermodynamic quantity.

A very preliminary results on the energy and the system size dependence of the $\Phi_{p_t}^{(3)}$ are presented in Figs. 8 and 9, respectively. They show the measured points for different charge particles along with the systematic errors (shaded area) caused by the limited two-track resolution which influences the measured fluctuations. The methods of estimation the statistical and systematic errors from Φ_{p_t} stability for different event and track selection criteria can be found in our previous paper [31].

For all three charge combinations a visible energy and system size dependencies of the $\Phi_{p_t}^{(3)}$ are observed. They increase towards lower values of freeze-out points ($\mu_B \approx 250$ MeV and $T \approx 160$ MeV). It should be noted that this values are close to those parameters where the critical point effect was early observed in the system size dependence of mean p_t and multiplicity fluctuations with $\Phi_{p_t}^{(2)}$ and ω measures, respectively.

Moreover, an increase of the $\Phi_{p_t}^{(3)}$ values from pp to PbPb collisions and its maximum at 158 AGeV is qualitatively quite similar to the early quoted $\Phi_{p_t}^{(2)}$ results for small p_t [38], which confirm the expectation that fluctuations due to the proximity to the critical point originate mainly from low p_t pions. For further study of higher moment fluctuations the progress in data analysis and the relevant theoretical predictions are necessary.

4.3. Fluctuations of azimuthal particle distributions

Event-by-event fluctuations and correlations in azimuthal angle are currently widely investigated in various experiments. They were proposed to investigate plasma instabilities [44], search for the critical point and onset of deconfinement, and measure fluctuations of elliptic

flow [45, 46]. For this study the Φ measure is chosen as it is a strongly intensive measure of fluctuations (does not depend on volume and on the volume fluctuations). Earlier used to evaluate fluctuations in transverse momentum this measure is now applied to azimuthal angle ϕ:

$$\Phi_\phi = \sqrt{\frac{\langle Z_\phi^2 \rangle}{\langle N \rangle}} - \sqrt{\overline{z_\phi^2}}. \tag{7}$$

There are several other effects that influence the values of this measure, such as resonance decay, momentum conservation, flow and quantum statistics. Several models were employed to test separately the influence of these physics effects. In addition, properties of this Φ_ϕ function are investigated through fast generators and with complex models such as Pythia, Hijing, and UrQMD.

Preliminary results of NA49 on Φ_ϕ [47] are illustrated in Fig. 10.

Fig. 10*a* shows the energy dependence of Φ_ϕ (20–158 AGeV) for the 7.2% most central PbPb interactions. There is no signifucant energy dependence, however negatively charged particles show positive Φ_ϕ values. The results from UrQMD, obtained with the same kinematic restrictions, show values consistent with zero. In the simulation the limited NA49 acceptance causes a major reduction in the absolute value of the Φ_ϕ measure. The main effect is due to the rapidity cut.

Fig. 10*b* presents the system size dependence of Φ_ϕ derived from the data for *pp*, CC, SiSi, and 6 centralities of PbPb collision at the highest SPS energy (158 AGeV). Significant positive values of Φ_ϕ are observed with a maximum for peripheral PbPb interactions. This is qualitatively similar to the results obtained by NA49 for average p_t [31] and multiplicity [33] fluctuations. Further studies are planned to understand these intriguing effects.

4.4. Particle ratio fluctuations

Hadron yield ratios characterize the chemical composition of the fireball in each event and the event-by-event fluctuations of the conserved quantities such as net baryon number and strangeness are sensitive to the properties of the early stage of the nucleus collisions.

In addition to the hadron production properties observed at the phase transition several models suggest the study of hadron ratio fluctuations to gain further insight into the nature of the deconfinement phase transition. Particle ratio fluctuations might also be affected

by the critical point. Moreover, these fluctuations are less strongly affected by hadronic reinteractions in the later stage of the collisions.

The measurement of hadron ratio fluctuations by NA49 is expressed in terms of dynamical fluctuations $\sigma_{\rm dyn}$ which referees to those fluctuations remaining after removing fluctuations from finite number statistics as well as effects from detector resolution and particle identification. The dynamical fluctuation is defined as

$$\sigma_{\rm dyn} = sign(\sigma^2_{\rm data} - \sigma^2_{\rm mix})\sqrt{\mid \sigma^2_{\rm data} - \sigma^2_{\rm mix} \mid} \, . \tag{8}$$

.

It measures the difference between widths of the particle ratio distributions for data $\sigma_{\rm data}$ and for artificially produced mixed events $\sigma_{\rm mix}$.

Fig. 11 shows preliminary results on the dynamical event-by-event fluctuations $\sigma_{\rm dyn}$ of the K/π, p/π, and K/p ratios for SPS (NA49) [48–50] and RHIC (STAR) [51, 52] energies.

In Fig. 11*a* a positive value of $\sigma_{\rm dyn}$ for K/π ratio is observed for the whole energy range and it is almost constant from top SPS to RHIC energies , whereas the steep rise of the K/π fluctuations is indicated towards lower SPS energies. As shown in [53] this feature could be considered as a signal for the onset of deconfinement. When comparing these measurements to the predictions of the transport models UrQMD [54, 55] and HSD [56] one finds large differences between the model predictions and failure to reproduce data in a whole energy range.

Fig. 11*b* illustrates $\sigma_{\rm dyn}$ for the p/π ratio fluctuations. It is reproduced by hadronic models in the SPS energy range and can be understood as an effect of the nucleon resonance decay.

The K/p ratio fluctuations are shown in Fig. 11*c*. The smooth behavior of the negative $\sigma_{\rm dyn}$ at RHIC and almost all SPS energies sharply changes to the significant positive value at the lowest SPS energy of 20 AGeV. Comparing the results with the UrQMD calculations one finds again that the model does not describe the overall energy dependence of the K/p ratio fluctuation, in particular, the enhanced value of $\sigma_{\rm dyn}$ at 20 AGeV as well as the RHIC energy points. Furthermore, it is visible that applying different acceptances (in our case, those for the NA49 and STAR experiments) the model calculations do not change the predictions for all above three particle ratio fluctuations.

5. SUMMARY AND CONCLUSIONS

Experiments of NA49 at CERN SPS motivated by predictions of the Statistical Model of the Early Stage indicate that deconfinement starts to occur at the early stage of central PbPb collisions for beam energies above ~ 30 AGeV.

The NA49 also searched for indications of of the predicted QCD critical point where an enhanced event-by-event multiplicity and mean transverse momentum fluctuations are expected. The results from energy scan (variation of baryonic chemical potential μ_B) in central PbPb collisions show no evidence for the expected critical point location at $\mu_B \approx 360$ MeV and $T_{\rm chem} \approx 150$ MeV, while a visible fluctuations are seen in system size dependence (variation of temperature $T_{\rm chem}$) for relatively lighter systems produced in 158 AGeV CC and SiSi collisions at $\mu_B \approx 250$ MeV and $T_{\rm chem} \approx 160$ MeV.

A very preliminary analysis of the having advantage higher moment fluctuations using $\Phi^{(3)}_{p_t}$ measure exhibits a visible effect and has to be continued.

The azimuthal angle fluctuations of charged particles were analyzed using the Φ_ϕ measure. The measurements for central PbPb collisions show weak energy dependence of Φ_ϕ. However, in the system size dependence the significant rise of the measured fluctuations towards a smaller colliding systems are indicated. This is qualitatively similar to the mean transverse momentum and multiplicity fluctuation results obtained in NA49.

The NA49 results on the energy dependence of event-by-event hadron ratio fluctuations do not rise to a coherent interpretation. While the p/π ratio fluctuations can be understood in terms of resonance decay and are reproduced by hadronic models, there are distinctive interpretation of the excitation function of K/π and K/p ratio fluctuations which remain to be settled. They show an interesting effects, i.e. an increase of K/π ratio fluctuation with decreasing the collision energy, change the sign and jump at the lowest SPS energy of 20 AGeV. The relations of these features to the onset of deconfinement still has to be understood.

A further detailed energy and system size scan to investigate the properties of the onset of deconfinement and to establish the existence of the QCD critical point will be performed in the NA61/SHINE experiment at the CERN SPS in order to cover a broad range of the phase diagram.

6. ACKNOWLEDGMENTS

This work was supported by the US Department of Energy Grant DE-FG03-97ER41020/A000, the Bundesministerium fur Bildung and Forschung, Germany, the Virtual Institute VI-146 of Helmholtz Gemeinschaft, Germany, the Polish Ministry of Science and High Education (1 P03B 006 30, 1 P03B 127 30, 0297/B/H03/2007/33, N N202 078735, N N202 204638), the Hungarian Scientific Research Foundation (T032648, T032293, T043514), the Hungarian National Science Foundation, OTKA, (F034707), the Bulgarian National Science Fund (Ph-09/05), the Croatian Ministry of Science, Education and Sport (Project 098-0982887-2878), Stichting FOM, the Netherlands, and the Deutsche Forschungsgemeinschaft (DFG).

---

1. T. Alber *et al.* (NA49 Collab.), Phys. Rev. Lett. **75**, 3814 (1995).
2. U. Heinz and M. Jacob, arXiv: nucl-th/0002042.
3. M. Gaździcki and M. I. Gorenstein, Acta Phys. Polon. B **30**, 2705 (1999).
4. C. Alt *et al.* (NA49 Collab.), Phys. Rev. C **77**, 024903 (2008).
5. M. Gaździcki, J.Phys. G **30**, S701 (2004).
6. P. Seyboth *et al.*, Acta Phys. Polon. B **37**, 3429 (2006).
7. V. Friese (NA49 Collab.), PoS CPOD09, 005 (2009); arXiv: 0908.2720 [nucl-ex].
8. Z. Fodor and S. D. Katz, JHEP **0404**, 050 (2004).
9. P. Braun-Munzinger, J. Cleymans, H. Oeschler, and K. Redlich, Nucl. Phys. A **697**, 902 (2002); P. Braun-Munzinger and J. Stachel, J.Phys. G **28**, 1971 (2002).
10. F. Becattini, J. Manninen, and M. Gaździcki, Phys. Rev. C **73**, 044905 (2006).
11. F. Becattini *et al.*, Phys. Rev. C **69**, 024905 (2004).
12. M. Stepanov, K. Rajagopal, E. Shuryak, Phys. Rev. D **60**, 114028 (1999).
13. V. Koch, arXiv: 0810.2520 [nucl-th].
14. S. Afanasiev *et al.* (NA49 Collab.), Nucl. Instrum. Methods. A **430**, 210 (1999).
15. H. Sorge, H. Stocker, and W. Greiner, Nucl. Phys. A **498**, 567 (1989).
16. S. A. Bass *et al.*, Prog. Part. Nucl. Phys. **41**, 255 (1998).
17. E. L. Bratkovskaya *et al.*, Phys. Rev. C **69**, 054907 (2004).

18. A. Andronic, P. Braun-Munzinger, and J. Stachel, Nucl. Phys. A **772**, 167 (2006).
19. A. Andronic, P. Braun-Munzinger, and J. Stachel, Acta Phys. Polon. B **40**, 1005 (2009).
20. M. Gaździcki *et al.*, Braz. J. Phys. **34**, 322 (2004).
21. H. Petersen and M. Bleicher, PoS CPOD2006, 025 (2006); arXiv: nucl-th/0611001.
22. S. V. Akkelin and Yu. M. Sinyukov Phys. Rev. C **73**, 034908 (2006).
23. L. Kumar *et al.* (STAR Collab.), J. Phys. G **36**, 064066 (2009).
24. G. Wang *et al.* (STAR Collab.), Nucl. Phys. A **830**, 19c (2009).
25. D. Cebra *et al.* (STAR Collab.), arXiv: 0903.4702.
26. K. Rajagopal and F. Wilczek, arXiv: hep-ph/0011333.
27. C. Bernard *et al.*, Phys. Rev. D **75**, 094505 (2007).
28. O. Scavenius *et al.*, Phys. Rev. C **64**, 045202 (2001).
29. R. V. Gavai and S. Gupta, Phys. Rev. D **78**, 114503 (2008).
30. M. Gaździcki and St. Mrówczyński, Z.Phys. C **54**, 127 (1992).
31. T. Anticic *et al.* (NA49 Collab.), Phys. Rev. C **70**, 034902 (2004).
32. T. Anticic *et al.* (NA49 Collab.), Phys. Rev. C **79**, 044904 (2009).
33. C. Alt *et al.* (NA49 Collab.), Phys. Rev. C **75**, 064904 (2007).
34. C. Alt *et al.* (NA49 Collab.), Phys. Rev. C **78**, 034914 (2008).
35. B. Lungwitz, PhD thesis (2008), http://edms.cern.ch/document/989055/1.
36. V. P. Konchakovski *et al.*, Phys. Rev. C **73**, 034902 (2006).
37. K. Grebieszkow *et al.* (NA49 Collab.), arXiv: 0907.4101 [nucl-ex].
38. K. Grebieszkow *et al.* (NA49 and NA61 Collabs.), arXiv: 0909.0485 [hep-ex].
39. M. Stepanov, private communications.
40. Y. Hatta and T. Ikeda, Phys. Rev. D **67**, 014028 (2003).
41. St. Mrówczyński, Phys. Lett. B **465**, 8 (1999).
42. M. A. Stepanov, Phys. Rev. Lett. **102**, 032301 (2009).
43. M. Cheng *et al.*, Phys. Rev. D **79**, 074505 (2009); arXiv: 0811.1006 [hep-lat].
44. St. Mrówczyński, Phys. Lett. B **314**, 118 (1993).
45. St. Mrówczyński and E. V. Shuryak, Acta Phys. Polon. B **34**, 4241 (2003).
46. M. Miller and R. Snellings, arXiv: nucl-ex/0312008.
47. T. Cetner, K. Grebieszkow *et al.* (NA49 Collab.), arXiv: 1008.3412 [nucl-ex].
48. T. Schuster *et al.* (NA49 Collab.), PoS **CPOD2009**, 029 (2009).

49. D. Kresan *et al.* (NA49 Collab.), PoS CPOD2009, 031 (2009).
50. C. Alt *et al.* (NA49 Collab.), Phys. Rev. C **79**, 044910 (2009).
51. B. I. Abelev *et al.* (STAR Collab.), Phys. Rev. Lett. **103**, 092301 (2009).
52. J. Tian *et al.* (STAR Collab.), J. Phys. G **37**, 094044 (2010).
53. M. I. Gorenstein, M. Gaździcki, and O. S. Zozulya, Phys. Lett. B **585**, 237 (2004).
54. M. Bleicher *et al.*, J. Phys. G **25**, 1859 (1999); H. Petersen, M. Bleicher, S. A. Bass, and H. Stocker, arXiv: 0805.0567 [hep-ph].
55. H. Wang, private communications.
56. V. P. Konchakovski, M. Hauer, M. I. Gorenstein, and E. L. Bratkovskaya, J. Phys. G **36**, 125106 (2009).

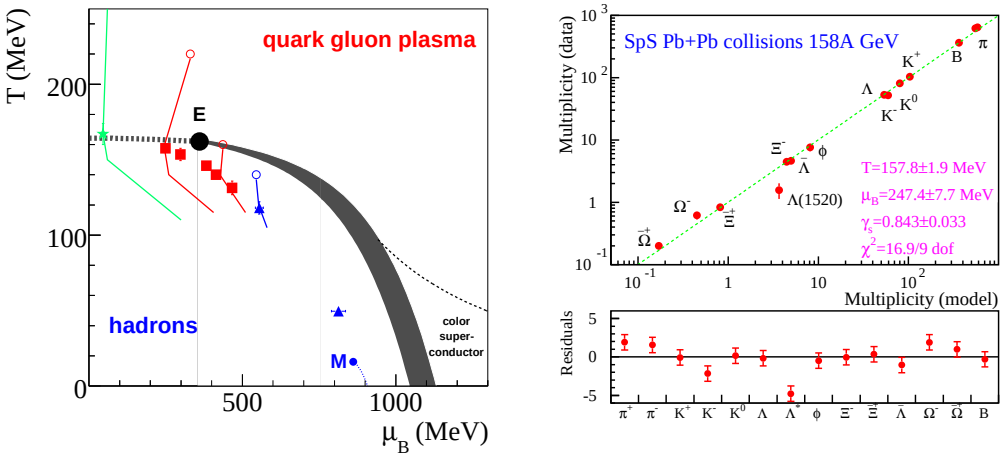

Figure 1. (a): Phase diagram of strongly interacting matter in the plane temperature (T) versus barionic chemical potential (μ_B). The dark band is a lattice QCD estimate [8] of the first order phase boundary between quark-gluon plasma (OGP) and hadrons which ends in a critical point E and then proceeds to a crossover. Symbols denote the chemical freeze-out parameters of heavy ion collisions at different energies as extracted by statistical model fits [9–11] to the data of the hadron composition at RHIC (STAR), SPS (NA49), AGS, and SIS. The open symbols schematically indicate possible values of initial parameters of the reaction systems, which then might evolve along paths as depicted by the vertical lines.

(b): Results of a statistical model fit to NA49 hadron yields in 158 AGeV central PbPb collisions [11].

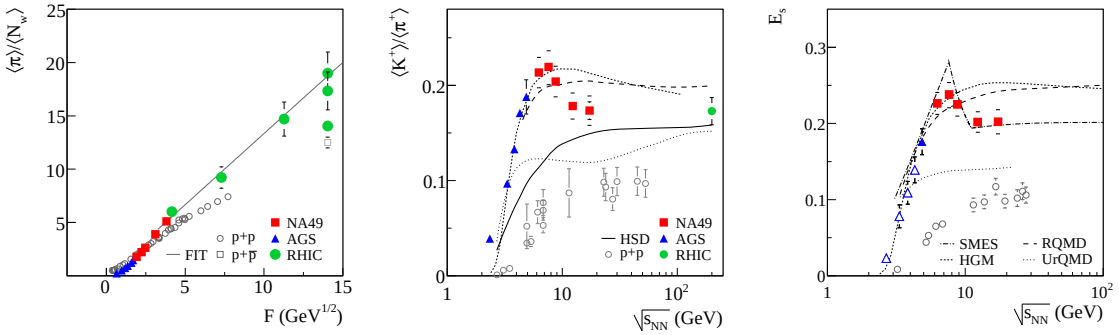

Figure 2. (a): Total pion yield in a full phase space (4π) per wounded nucleons as a function of the Fermi variable $F \approx \sqrt{s_{NN}^{1/2}}$.

(b): Energy dependence of the $\langle \mathrm{K}^+ \rangle / \langle \pi^+ \rangle$ ratio in full phase space.

(c): Ratio E_S of total number of strangeness carriers to entropy (pions) versus collision energy. NA49 results in PbPb collisions [4] are shown together with the data in AA collisions at lower and higher energies, and compared to the measurements in *pp* reactions. Curves show model predictions.

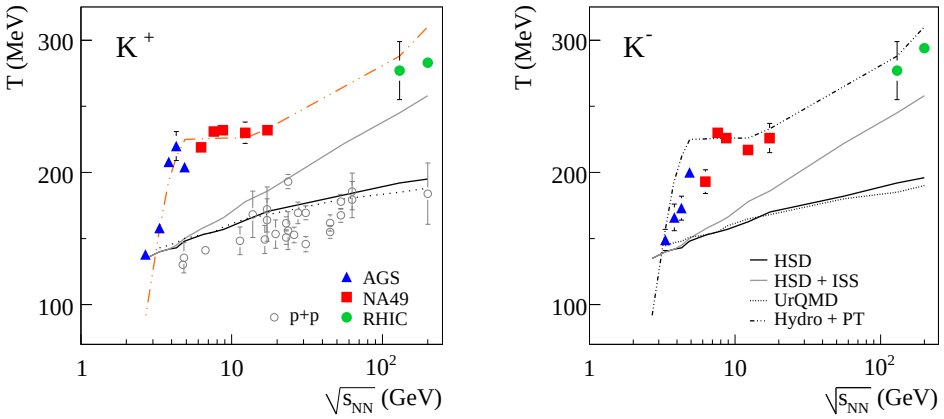

Figure 3. Energy dependence of the inverse slope parameter T of transverse mass spectra for K^+ (a) and K^- (b) [4]. The data are compared to results of UrQMD [16] and HSD [17] models, and hydrodynamical model (Hydro+PT) [20] incorporating the first order phase transition.

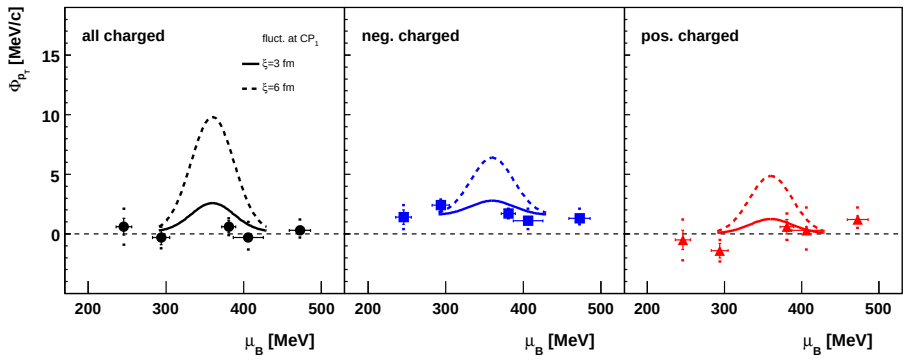

Figure 4. Energy (μ_B) dependence of transverse momentum fluctuation measure Φ_{p_t} for the 7.2% most central PbPb collisions [32] in the forward-rapidity region and $0.005 < p_t < 1.5$ GeV/c. The values of baryochemical potential μ_B were taken from statistical hadron gas model fits to particle yields [10] at each collision energy. Curves indicate predictions for the estimated critical point CP_1 (see text).

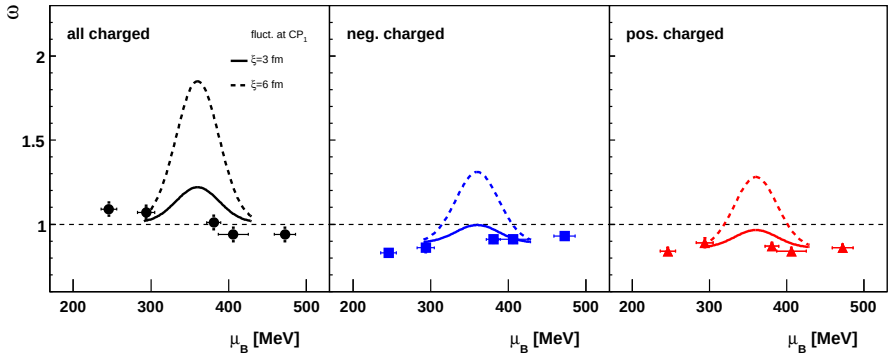

Figure 5. Energy (μ_B) dependence of multiplicity fluctuations, scaled variance ω, for the 1% most central PbPb collesions [34] in the forward-rapidity region. Curves indicate predictions for the CP_1 (see text). The values of baryochemical potential μ_B were taken from statistical hadron gas model fits to particle yields [10] at each collision energy.

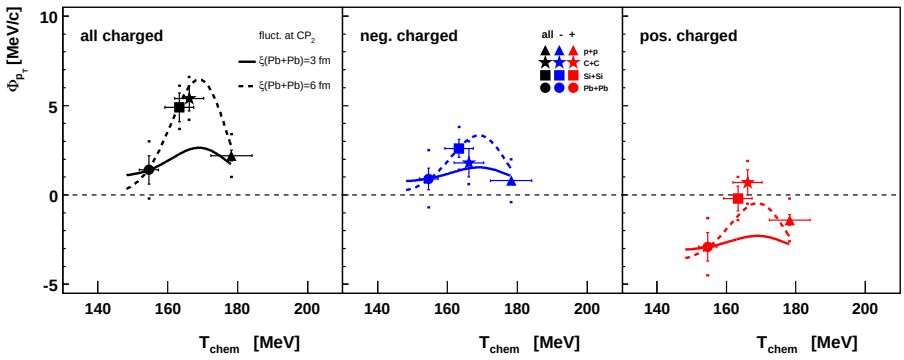

Figure 6. System size ($T_{\rm chem}$) dependence of transverse momentum fluctuation measure Φ_{p_t} at 158 AGeV from data for pp, semi-central CC (15.3%) and SiSi (12.2%), and the 5% most central PbPb collisions [31] in forward-rapidity region. Curves indicate predictions for critical point CP_2 (see text) shifted to reproduce the Φ_{p_t} values for central PbPb collisions.

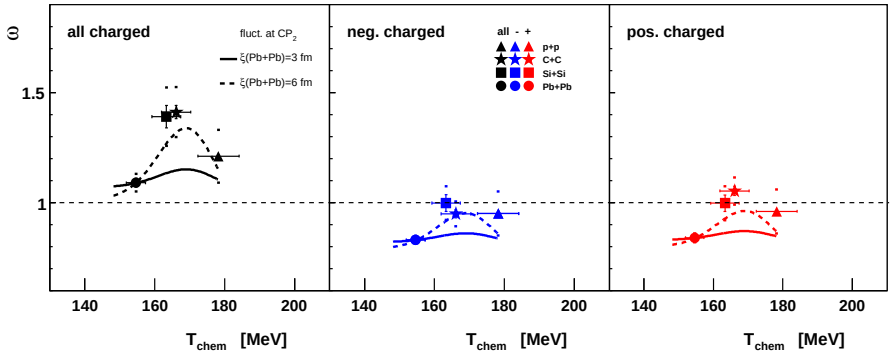

Figure 7. System size ($T_{\rm chem}$) dependence of multiplicity fluctuations, scaled variance ω, at 158 AGeV for pp [33], the 1% most central CC, SiSi [35], and PbPb collisions [34] in forward rapidity region. Curves indicate predictions for ctitical point CP_2 (see text) shifted to reproduce the ω values for central PbPb collisions.

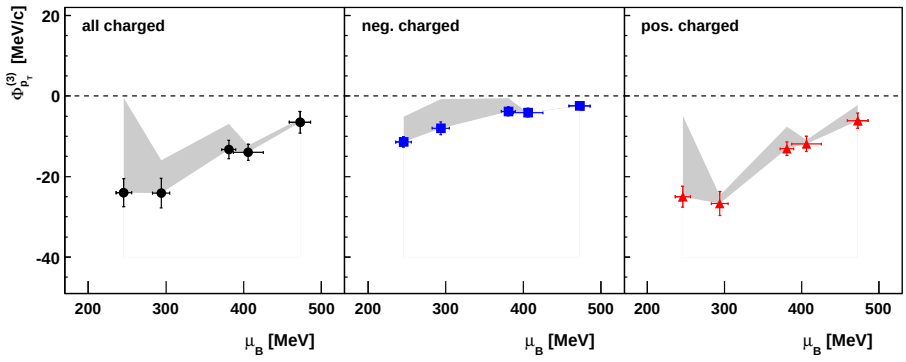

Figure 8. NA49 very preliminary. Energy (μ_B) dependence for the third moment $\Phi^{(3)}_{p_t}$ of transverse momentum fluctuations for the 7.2% most central PbPb collisions at 20, 30, 40, 80, and 158 AGeV in the forward-rapidity region and $0.005 < p_t < 1.5$ GeV/c. The shaded area corresponds to the estimated systematic errors .

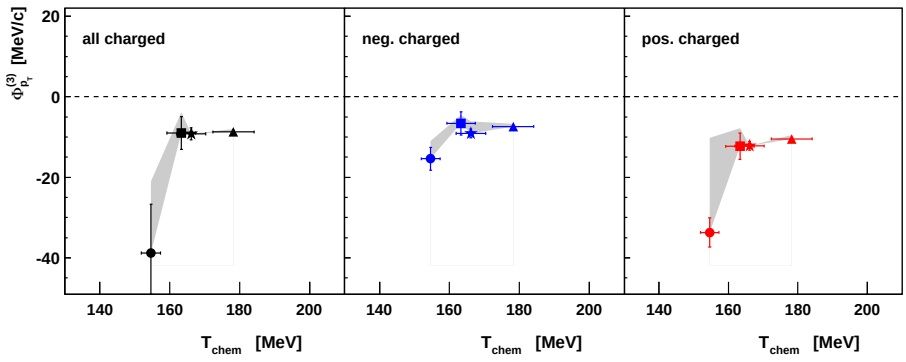

Figure 9. NA49 very preliminary. System size ($T_{\rm chem}$) dependence for the third moment $\Phi^{(3)}_{p_t}$ of transverse momentum fluctuations at 158 AGeV derived from the data for pp, semi-central CC (15.3%), SiSi (12.2%), and the 5% most central PbPb collisions in forward-rapidity region. The shaded area corresponds to the estimated systematic errors.

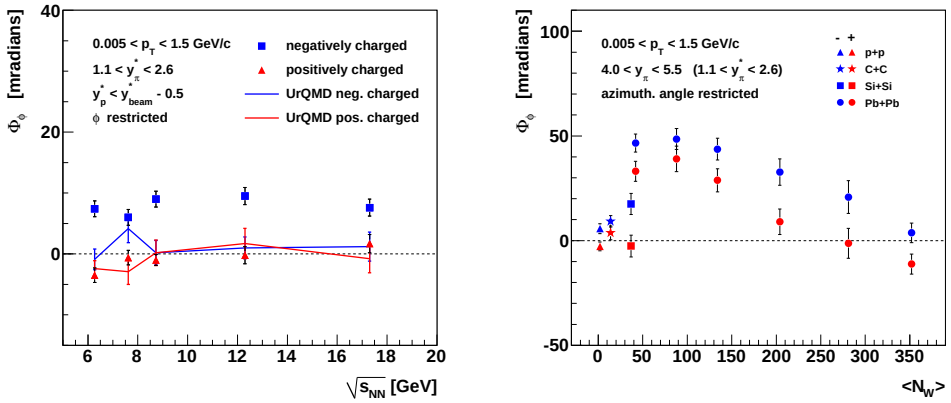

Figure 10. (a): Energy dependence of the azimuthal angle fluctuation measure Φ_ϕ for the 7.2 % most central PbPb interactions. The data are compared to UrQMD calculations.

(b): System size dependence of Φ_ϕ derived from data for *pp*, CC, SiSi, and 6 centralities of PbPb interactions at 158 AGeV.

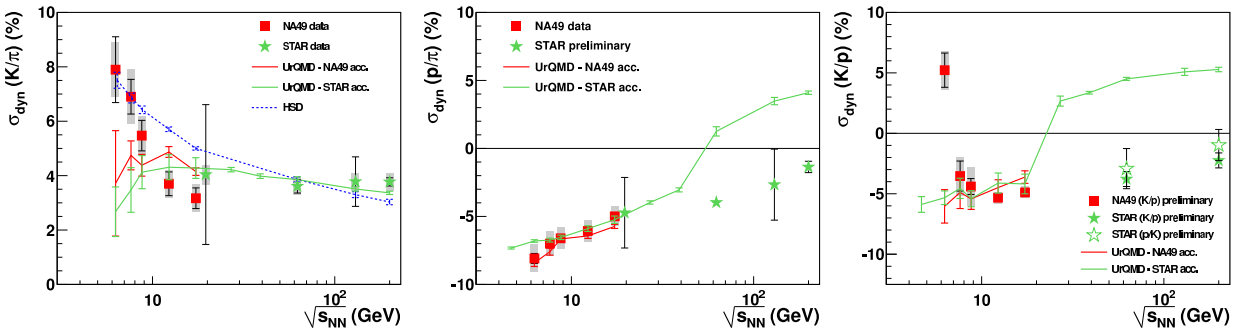

Figure 11. Energy dependence of the event-by-event dynamical fluctuations $\sigma_{\rm dyn}$ for the p/π (a), K/π (b) and K/p (c) ratios. Data from NA49 [48–50] and STAR [51, 52] results are compared to the UrQMD [54, 55] and HSD [56] model calculations..

FIGURE CAPTIONS

Fig. 1: (a): Phase diagram of strongly interacting matter in the plane temperature (T) versus baryonic chemical potential (μ_B). The dark band is a lattice QCD estimate [8] of the first order phase boundary between quark-gluon plasma (QGP) and hadrons which ends in a critical point E and then proceeds to a crossover. Symbols denote the chemical freeze-out parameters of heavy ion collisions at different energies as extracted by statistical model fits [9–11] to the data of the hadron composition at RHIC (STAR), SPS (NA49), AGS, and SIS. The open symbols schematically indicate possible values of initial parameters of the reaction systems, which then might evolve along paths as depicted by the vertical lines.

(b): Results of a statistical model fit to NA49 hadron yields in 158 AGeV central PbPb collisions [11].

Fig. 2: (a): Total pion yield in a full phase space (4π) per wounded nucleons as a function of the Fermi variable $F \approx \sqrt{s_{NN}^{1/2}}$.

(b): Energy dependence of the $\langle \mathrm{K}^+ \rangle / \langle \pi^+ \rangle$ ratio in full phase space.

(c): Ratio E_S of total number of strangeness carriers to entropy (pions) versus collision energy. NA49 results in PbPb collisions [4] are shown together with the data in AA collisions at lower and higher energies, and compared to the measurements in pp reactions. Curves show model predictions.

Fig. 3: Energy dependence of the inverse slope parameter T of transverse mass spectra for K^+ (a) and K^- (b) [4]. The data are compared to results of UrQMD [16] and HSD [17] models, and hydrodynamical model (Hydro+PT) [20] incorporating the first order phase transition.

Fig. 4: Energy (μ_B) dependence of transverse momentum fluctuation measure Φ_{p_t} for the 7.2% most central PbPb collisions [32] in the forward-rapidity region and $0.005 < p_t < 1.5$ GeV/c. The values of baryochemical potential μ_B were taken from statistical hadron gas model fits to particle yields [10] at each collision energy. Curves indicate predictions for the estimated critical point CP_1 (see text).

Fig. 5: Energy (μ_B) dependence of multiplicity fluctuations, scaled variance ω, for the 1% most central PbPb collesions [34] in the forward-rapidity region. Curves indicate predictions

for the CP_1 (see text). The values of baryochemical potential μ_B were taken from statistical hadron gas model fits to particle yields [10] at each collision energy.

Fig. 6: System size ($T_{\rm chem}$) dependence of transverse momentum fluctuation measure Φ_{p_t} at 158 AGeV from data for *pp*, semi-central CC (15.3%) and SiSi (12.2%), and the 5% most central PbPb collisions [31] in forward-rapidity region. Curves indicate predictions for critical point CP_2 (see text) shifted to reproduce the Φ_{p_t} values for central PbPb collisions.

Fig. 7: System size ($T_{\rm chem}$) dependence of multiplicity fluctuations, scaled variance ω, at 158 AGeV for *pp* [33], the 1% most central CC, SiSi [35], and PbPb collisions [34] in forward rapidity region. Curves indicate predictions for ctitical point CP_2 (see text) shifted to reproduce the ω values for central PbPb collisions.

Fig. 8: NA49 very preliminary. Energy (μ_B) dependence for the third moment $\Phi^{(3)}_{p_t}$ of transverse momentum fluctuations for the 7.2% most central PbPb collisions at 20, 30, 40, 80, and 158 AGeV in the forward-rapidity region and $0.005 < p_t < 1.5$ GeV/c. The shaded area corresponds to the estimated systematic errors .

Fig. 9: NA49 very preliminary. System size ($T_{\rm chem}$) dependence for the third moment $\Phi^{(3)}_{p_t}$ of transverse momentum fluctuations at 158 AGeV derived from the data for *pp*, semi-central CC (15.3%), SiSi (12.2%), and the 5% most central PbPb collisions in forward-rapidity region. The shaded area corresponds to the estimated systematic errors.

Fig. 10: (a): Energy dependence of the azimuthal angle fluctuation measure Φ_ϕ for the 7.2 % most central PbPb interactions. The data are compared to UrQMD calculations.

(b): System size dependence of Φ_ϕ derived from data for *pp*, CC, SiSi, and 6 centralities of PbPb interactions at 158 AGeV.

Fig. 11: Energy dependence of the event-by-event dynamical fluctuations $\sigma_{\rm dyn}$ for the p/π (a), K/π (b) and K/p (c) ratios. Data from NA49 [48–50] and STAR [51, 52] results are compared to the UrQMD [54, 55] and HSD [56] model calculations..